GENERAL INSTRUCTIONS

- **Authors: When accessing and uploading your corrections at the Author Gateway, please note we cannot accept new source files as corrections for your article. Do not send new Latex, Word, or PDF files, as we cannot simply "overwrite" your article. Please submit your corrections as an annotated PDF or as clearly written list of corrections, with location in article, using line numbers provided on your proof. You can also upload revised graphics to the Gateway.**
- **Authors: Please note that once you click "approve with no changes," the proofing process is now complete and your article will be sent for final publication and printing. Once your article is posted on Xplore, it is considered final and the article of record. No further changes will be allowed at this point so please ensure scrutiny of your final proof.**
- **Authors: Unless invited or otherwise informed, overlength page charges of $260 per page are mandatory for each page in excess of seven printed pages and are required for publication. If you have any questions regarding overlength page charges, need an invoice, or have any other billing questions, please contact reprints@ieee.org as they handle these billing requests.**

QUERY

Q1. Author: Please confirm or add details for any funding or financial support for the research of this article.

High-Resolution Chirped-Pulse ϕ-OTDR by Means of Sub-Bands Processing

Leonardo Marcon, Marcelo A. Soto, Miguel Soriano-Amat, Luis Costa, Maria R. Fernandez-Ruiz, Hugo F. Martins, Luca Palmieri, and Miguel Gonzalez-Herraez

***Abstract*—Conventional chirped-pulse (CP) phase-sensitive optical time-domain reflectometry (CP ϕ-OTDR) allows the interrogation of tens of kilometers of optical fiber with high accuracies of millikelvin or nanostrain. With respect to standard coherent-detection ϕ-OTDR, it shows increased robustness to coherent fading and allows a linear and quantitative monitoring of the perturbations acting on the fiber. Its spatial resolution, however, remains a critical parameter and new techniques allowing its improvement without reducing significantly other performances (or increasing the setup complexity) are constantly being researched. In this paper, we propose a method to improve the spatial resolution of CP ϕ-OTDR without reducing the input pulse width, by means of sub-bands processing. The method is based on adding an optical carrier to the input pulse. Using digital filtering, the spectrum of the fiber backscatter can be split into multiple sub-bands. Each of these sub-bands corresponds to the fiber response generated by a short optical pulse, chirped over a smaller frequency range. This way each sub-band results in ϕ-OTDR measurements with high spatial resolution, but with a reduced SNR. A dedicated post-processing methodology is proposed to mitigate the SNR reduction obtained from each sub-band, while securing high-resolution measurements of the perturbations acting on the fiber. Experimental results demonstrate the possibility of achieving CP ϕ-OTDR measurements with a 15-fold spatial resolution improvement over the conventional CP analysis, at the expense of an SNR reduction lower than a factor 2.**

***Index Terms*—Digital signal processing, phase-sensitive optical time-domain reflectometry, Rayleigh scattering.**

Manuscript received October 31, 2019; revised January 16, 2020 and March 4, 2020; accepted March 14, 2020. Date of publication; date of current version. This work was supported in part by Project FINESSE MSCA-ITN-ETN-722509, in part by the DOMINO Water JPI project under the WaterWorks2014 cofounded call by EC Horizon 2020, in part by ERANET Cofund Water Works 2014 call, Spanish MINECO and Italian MIUR, in part by Comunidad de Madrid and
Q1 FEDER Program under Grant SINFOTON2-CM: P2018/NMT-4326, and in part by MINECO under Project RTI2018-097957-B-C31. The work of Leonardo Marcon was supported by Fondazione Ing. Aldo Gini. Marcelo A. Soto was supported in part by AC3E ANID-Basal Project FB0008 and in part by "Becas Iberoamérica Santander Universidades Convocatoria 2018" (research stay at Universidad de Alcalá, Spain). The work of Maria R. Fernandez-Ruiz and Hugo F. Martins were supported by the Spanish Ministerio de Ciencia, Innovación y Universidades (CIENCIA) under Contracts FJCI-2016-27881 and IJCI-2017-33856. (*Corresponding author: Leonardo Marcon*.)

Leonardo Marcon and Luca Palmieri are with the Department of Information Engineering, University of Padova, 35131 Padova, Italy (e-mail: leonardo.marcon.1@phd.unipd.it; luca.palmieri@dei.unipd.it).

Marcelo A. Soto is with the Department of Electronic Engineering, Universidad Técnica Federico Santa María, 2390123 Valparaíso, Chile (e-mail: marcelo.sotoh@usm.cl).

Miguel Soriano-Amat, Luis Costa, Maria R. Fernandez-Ruiz, and Miguel Gonzalez-Herraez are with the Departamento de Electronica, Universidad de Alcalá, Edificio Politécnico, 28871 Madrid, Spain (e-mail: miguel.soriano@uah.es; ldpcosta@gmail.com; rosario.fernandezr@uah.es; miguel.gonzalezh@uah.es).

Hugo F. Martins is with the Instituto de Óptica "Daza de Valdés", IO-CSIC, 28006 Madrid, Spain (e-mail: h.fidalgo@uah.es).

Color versions of one or more of the figures in this article are available online at http://ieeexplore.ieee.org.

Digital Object Identifier 10.1109/JLT.2020.2981741

I. Introduction

DISTRIBUTED acoustic sensors (DAS) based on Rayleigh backscattering have become fundamental elements for safety applications [1], [2], particularly in harsh environments. The possibility of performing the analysis either in time-domain or frequency-domain guarantees flexible performance between coarse long-range [3] and accurate short-range [4] monitoring.

Phase-sensitive optical time-domain reflectometry (ϕ-OTDR) [5] is one of the most common DAS configurations due to its good performance and reduced cost. It requires a pulsed coherent light source that allows the interrogation of tens of kilometers of optical fiber with an acoustic bandwidth of few kilohertz and a spatial resolution proportional to the launched pulse width. The amplitude and temporal width of the optical pulses determine the amount of power backscattered from the fiber so, to guarantee a sufficient signal to noise ratio (SNR) in the measurement, either the amplitude must be increased, or long pulses must be used. The onset of nonlinear phenomena like modulation instability [6] imposes strong limits to the maximum pulse amplitude allowed at the fiber input. This way, the use of long pulses, which may force spatial resolutions in the order of tens of meters, becomes unavoidable to obtain DAS measurements with high SNR. Therefore, the use of ϕ-OTDR is limited to those DAS applications where an accurate spatial monitoring is not necessary [7], [8].

In recent years, many efforts have been made to reduce the drawbacks of ϕ-OTDR setups, specifically coherent fading [9] and its nonlinear response to the perturbations acting on the fiber [10]–[12]. By introducing a linear chirp into the input pulse, such drawbacks can be strongly mitigated [13], [14]. The CP ϕ-OTDR setup guarantees a linear measurement of the perturbations, while securing an increased robustness to coherent fading and high temperature and strain resolutions (e.g., millikelvin and nanostrain levels) [15]. The spatial resolution, however, remains limited by the pulse width. Possible solutions for such issue can be found modifying the CP ϕ-OTDR setup into a TGD-OFDR [16], [17], or by using optical pulse coding [18] or wavelength-scanning coherent OTDR [19]. With these techniques sub-meter spatial resolutions have been achieved over long distances, at the cost of a higher complexity and cost [20].

In this paper, we propose a method based on sub-bands processing to improve the spatial resolution of the CP ϕ-OTDR, with minimal changes to the original setup and without reducing the width of the optical pulse. An optical carrier at a specific frequency is added to the interrogating pulse, allowing the extraction of the fiber response to the chirped pulse from the signal received at an intermediate frequency. By using digital filters, the spectrum of the fiber response is divided into multiple sub-bands, eventually overlapped, being conceptually analogous to the spectra of the fiber response generated by multiple slightly delayed short pulses. The analysis of any one of these sub-bands guarantees ϕ-OTDR traces characterized by high resolution but reduced SNR and shot-to-shot maximum measurable strain-temperature change. By performing an averaging operation during the analysis of the sub-bands, a mitigation of the SNR reduction can be achieved.

In this manuscript, starting from the description of the standard CP ϕ-OTDR setup and extending our preliminary results in [21], we derive a mathematical model of the backscattered response generated by an interrogation signal containing a linearly chirped pulse and an added optical carrier at a different frequency. We then describe the sub-bands processing, analyzing in detail the averaging operation used to mitigate the expectable SNR reduction obtained with this method. In addition, we propose an experimental setup to demonstrate the spatial resolution enhancement guaranteed by the sub-bands processing and we compare the results with those obtained from a standard CP ϕ-OTDR. By accepting a modest reduction of the measurement SNR and of the shot-to-shot maximum measurable strain-temperature change, experimental results demonstrate a 15-fold improvement of the spatial resolution. Finally, we discuss the advantages of overlapped sub-bands to increase the number of terms in the averaging operation and we optimize the process. To have a higher control over the fiber perturbed sections and to focus on the working principle of the propose method we used slow temperature changes as perturbations. No variation of the sensors dynamic capability should occur if a sufficient processing power is available.

II. Theoretical Model

In a standard CP ϕ-OTDR [18] the input pulse $P_{\text{std}}(t, z)$ can be defined as:

$$P_{\text{std}}(t,z) = E_0 \text{rect}\left[\frac{t-\beta_1(z)}{\tau_p}\right] P_{cp}(t,z) \tag{1}$$

where E_0 is the pulse field amplitude, $\beta_1(z) = \int_0^z n_g(z)dz/c$ is the propagation delay, τ_p is the pulse width and:

$$P_{cp}(t,z) = e^{j2\pi(\upsilon_0+\delta\upsilon/\tau_p[t-\beta_1(z)])(t-\beta_1(z))} \tag{2}$$

is the linearly chirped term with total applied chirp $\delta\upsilon$.

As $P_{\text{std}}(t, z)$ propagates along the fiber, it generates a Rayleigh backscattering signal that represents the fiber response to the chirped pulse. This response can be described as the convolution $*$ of the input pulse with the fiber Rayleigh backscattering profile function $r(z)$:

$$E_{\text{std}}(t) = P_{\text{std}}(t,z) * r(z). \tag{3}$$

Upon detection $E_{\text{std}}(t)$ is converted from the optical to the electrical domain, resulting in a photocurrent described as:

$$I_{\text{std}}(t) = E_{\text{std}}(t)\, E_{\text{std}}{}^{cc}(t) \tag{4}$$

where cc stands for complex conjugation and each time instant t can be associated with a fiber position z by $t = 2nz/c$.

When a perturbation acts on a position z_0 of the fiber, it induces a change Δn in the local refractive index [22]. Using a chirped pulse ϕ-OTDR to interrogate the fiber, in correspondence to the position z_0, Δn generates a linearly proportional longitudinal shift Λ of the local pattern of $I_{\text{std}}(t)$:

$$\frac{\Delta n}{n} = -\left(\frac{1}{\upsilon_0}\right)\left(\frac{\delta\upsilon}{\tau_p}\right)\Lambda, \tag{5}$$

which can be immediately translated into temperature or strain changes (e.g., ΔT or $\Delta\varepsilon$, respectively) through the relations [23]:

$$\left(\frac{1}{\upsilon_0}\right)\left(\frac{\delta\upsilon}{\tau_p}\right)\Lambda = 0.78\cdot\Delta\varepsilon,$$
$$\left(\frac{1}{\upsilon_0}\right)\left(\frac{\delta\upsilon}{\tau_p}\right)\Lambda = \left(6.92\cdot 10^{-6}\right)\cdot\Delta T. \tag{6}$$

By monitoring the longitudinal shifts in the pattern of $I_{\text{std}}(t)$ along the whole fiber, the local perturbations affecting the sensing fiber can be completely characterized.

A standard CP ϕ-OTDR interrogates the fiber with two identical pulses. Those pulses generate two traces, called reference $I_{std,r}(t)$ and measurement $I_{std,m}(t)$, obtained with a time difference δt. The shifts $\Lambda(t)$ over the temporal trace are calculated by a temporal cross-correlation operation $\star$ over a moving window along $I_{std,r}(t)$ and $I_{std,m}(t)$, defined by a correlation time $\tau_c \cong \tau_p$, which defines the spatial resolution:

$$I_{\text{xcorr}}(t) = I_{std,r}(t-\tau_c, t+\tau_c) \star I_{std,m}(t-\tau_c, t+\tau_c), \tag{7}$$

$$\Lambda(t) = \text{argmax}\left(I_{\text{xcorr}}(t)\right). \tag{8}$$

Using (6), $\Lambda(t)$ is converted to the corresponding ΔT or $\Delta\varepsilon$.

Any improvement in the spatial resolution of the CP ϕ-OTDR is hindered by the direct detection process in (4), which scrambles the spectral information contained in the fiber response to the chirped pulse $E_{\text{std}}(t)$. The easiest way to solve this issue and extract $E_{\text{std}}(t)$ consists in implementing a coherent receiver, but the necessity of a highly coherent laser, as well as the increased phase noise induced by the local oscillator and the need of polarization diversity in the receiver makes this alternative unappealing. To measure $E_{\text{std}}(t)$, we propose to modify the CP ϕ-OTDR interrogating signal in (1) by adding to the input pulse a separate optical carrier, so that:

$$P(t,z) = E_0 \text{rect}\left[\frac{t-\beta_1(z)}{\tau_p}\right]\left(P_{oc}(t,z) + P_{cp}(t,z)\right), \tag{9}$$

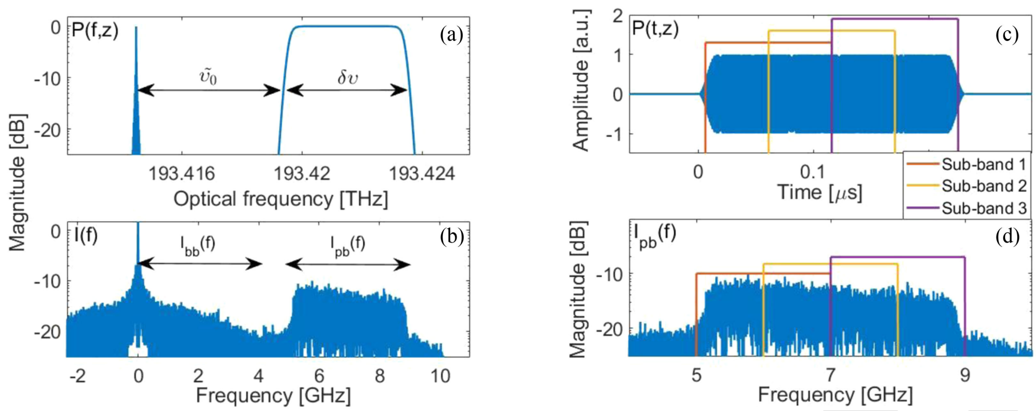

Fig. 1. (a) Optical spectrum of the input pulse $P(t,z)$, with $\delta\upsilon = 4$ GHz and $\widetilde{\upsilon_0} = 5$ GHz. (b) Electrical spectrum of the received backscattering signal $I(t)$ with highlighted baseband and passband terms. (c) Input optical pulse $P(t,z)$ with three overlapping sub-windows ($N = 2,\ F = 2$). (d) Pass-band term $I_{pb}(f)$ divided into three sub-bands. Each sub-band corresponds to the Rayleigh spectral response associated to one of the sub-windows in (c).

where:

$$P_{oc}(t,z) = e^{j2\pi(\upsilon_0-\widetilde{\upsilon_0})(t-\beta_1(z))},$$

$$P_{cp}(t,z) = e^{j2\pi(\upsilon_0+\delta\upsilon/\tau_p[t-\beta_1(z)])(t-\beta_1(z))}, \qquad (10)$$

are respectively the optical carrier at an optical frequency $\upsilon_0 - \widetilde{\upsilon_0}$, and the chirped pulse described in (2). Note that $P_{oc}(t,z)$ and $P_{cp}(t,z)$ have different central optical frequencies, as exemplified in Fig. 1(a). Due to the linearity of convolution, the propagation of the modified pulse $P(t,z)$ along the fiber can be modelled as the generation of two backscattering components:

$$E(t) = P(t,z) * r(z) = E_{oc}(t) + E_{cp}(t), \qquad (11)$$

and upon reception, the electrical signal becomes:

$$I(t) = E(t)E^*(t) = I_{bb}(t) + I_{pb}(t), \qquad (12)$$

where $I_{bb}(t) = |E_{oc}(t)|^2 + |E_{cp}(t)|^2$ and, by calling $\Re(\cdot)$ the real part operator, $I_{pb}(t) = 2\Re(E_{oc}(t)E_{cp}^*(t))$. As can be seen in Fig. 1(b), the spectrum $I_{bb}(f) = \mathcal{F}(I_{bb}(t))$ is a baseband, triangularly shaped term and, if we neglect the contribution of the added carrier, it corresponds to the spectrum of the signal received by the standard CP ϕ-OTDR in (4). The spectrum $I_{pb}(f) = \mathcal{F}(I_{pb}(t))$ is passband instead and, considering the optical carrier as a pure spectral line, it represents the fiber response to the chirped pulse $E_{cp}(t)$. Given that the spectral width of $I_{bb}(f)$ is twice the spectral width of $P_{cp}(t,z)$, the frequency shift in (9) must be at least $\widetilde{\upsilon_0} > \delta\upsilon$ to avoid overlaps with the spectrum of $I_{pb}(f)$. In the following analysis we will focus on $I_{pb}(f)$ which, assuming that the condition for the frequency shift $\widetilde{\upsilon_0}$ is satisfied, can be extracted from the received signal $I(f)$ by proper digital filtering. Due to the linear chirp applied to $P_{cp}(t,z)$, any sub-window of the input pulse in (9) generates a specific sub-band in $I_{pb}(f)$, as can be seen in Fig. 1(c) and 1(d). The spectrum of each sub-band corresponds to the spectrum generated when interrogating the fiber with a single short pulse, thus its analysis guarantees a sharp spatial resolution (i.e., improved with respect to the use of the entire chirped pulse), but at the cost of a reduced SNR and maximum shot-to-shot $\Lambda(t)$. The SNR reduction can be mitigated by exploiting the redundant information contained in the sub-bands: since they are extracted from the same pulse they correspond to simultaneous measurements of the same perturbations. The receiver noise affecting the different high-resolution ϕ-OTDR sections is uncorrelated, thus an averaging operation, accounting for the temporal shifts introduced during the sub-bands' extraction, can allow a strong SNR reduction mitigation while securing high spatial resolution measurements.

The measurement approach of the proposed scheme starts like the conventional CP ϕ-OTDR, by acquiring the reference $I_r(t)$ and measurement $I_m(t)$ traces at time instants separated by δt. Then, the corresponding bandpass components $I_{pb,r}(f)$ and $I_{pb,m}(f)$ are extracted using a digital band-pass filter of width $\delta\upsilon$. As mentioned above, the spatial resolution of an OTDR setup is proportional to the interrogating pulse width. Therefore, to improve the resolution by a factor N, it is necessary to split $I_{pb,r}(f)$ and $I_{pb,m}(f)$ into N independent sub-bands $I^n_{pb,r}(f)$, $I^n_{pb,m}(f),\ n = 1, \ldots N$, of width $\Delta W = \delta\upsilon/N$ and to adapt the correlation time accordingly $\widetilde{\tau_c} = \tau_p/N$. Each pair (reference and measurement) of sub-bands is converted to time-domain after synchronizing the filtering induced time shift:

$$I^n_{pb,r}(t) = \mathcal{F}^{-1}\left\{e^{-j2\pi f(n-1)\widetilde{\tau_c}} I^n_{pb,r}(f)\right\},$$

$$I^n_{pb,m}(t) = \mathcal{F}^{-1}\left\{e^{-j2\pi f(n-1)\widetilde{\tau_c}} I^n_{pb,m}(f)\right\}. \qquad (13)$$

The cross-correlation traces obtained from (7) are computed for each corresponding pair of $I^n_{pb,r}(t)$ and $I^n_{pb,m}(t)$, using the reduced correlation time $\widetilde{\tau_c}$ so that:

$$I^n_{\text{xcorr}}(t) = I^n_{pb,r}(t-\widetilde{\tau_c}, t+\widetilde{\tau_c}) \star I^n_{pb,m}(t-\widetilde{\tau_c}, t+\widetilde{\tau_c}) \quad (14)$$

and then averaged into a single one:

$$I_{\text{xcorr}}(t) = \frac{1}{N}\sum_{n=1}^{N} I^n_{\text{xcorr}}(t). \qquad (15)$$

The shifts $\Lambda(t)$ along the fiber are then extracted using the operation in (8) and converted to the corresponding temperature or strain change through the equations in (6).

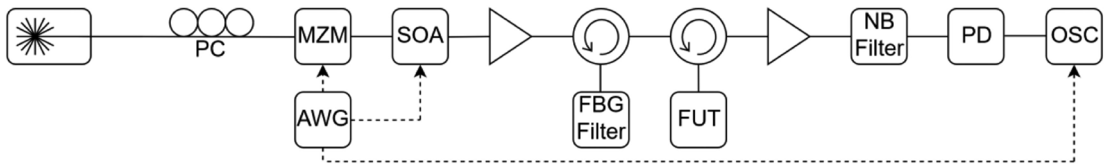

Fig. 2. Schematic representation of the experimental setup (the acronyms are explained in the text).

Averaging the cross-correlation traces $I^n_{\text{xcorr}}(t)$ as described in (15) is key for the operation of the proposed method to increase the spatial resolution of the CP ϕ-OTDR, as it mitigates the critical SNR reduction induced when dividing $I_{pb}(f)$ into sub-bands. The extraction of $\Lambda(t)$ in (8) works properly only when the central correlation peak is the highest, but if two traces with low SNR are used in (14), noise-induced side peaks at random lags may exhibit higher magnitudes. In such cases, $\Lambda(t)$ extracted from (8) is an outlier value and does not represent the perturbation affecting the fiber. Even after averaging all the shifts extracted from the N different correlation traces, the results will only be comparable (in terms of SNR) to the ones obtained using directly a single short pulse, thus generally with an SNR being too low to be useful. However, since the noise-induced side peaks in (1) appear at different lags for different cross-correlation traces, their amplitude can be significantly dampened by averaging $I^n_{\text{xcorr}}(t)$, allowing a correct extraction of the central correlation peak shift. It is not possible to use an arbitrary high value of N since a too low SNR and correlation time will generate chaotic results with no recoverable information. Since each sub-window corresponds to a shorter pulse, also the maximum $\Lambda(t)$ measurable shot-to-shot will be reduced. However, using standard parameters, such value will still be enough to monitor the vast majority of usual perturbations. The slight unevenness (<5 dB) of the band $I_{pb}(f)$ visible in Fig. 1(d) does not influence the quality of the results since the method is based on temporal cross-correlations. Such distortion will only impact slightly the amplitude of the correlation traces, but not the information of the temperature-strain perturbations contained in the temporal shift of the correlation peak.

So far, the description of the method has been based on the use of non-overlapping independent sub-windows, exhibiting uncorrelated noise that guarantees an efficient noise reduction by the averaging operation in (15). Such efficiency is reduced if partially overlapped sub-windows are used. This is because of the increased noise correlation; however, a larger number of terms available for averaging can compensate this effect, securing a good mitigation of the SNR reduction. Defining the shift between the central frequency of consecutive sub-bands as $\delta W = \Delta W/F$, with F being an integer number called overlap factor, $\tilde{N} = F(N-1)+1 > N$ partially overlapped sub-bands can be extracted setting $F > 1$. Since the noise of progressively overlapped sub-bands exhibits a growing correlation, the improvement provided by higher F value will saturate. The analysis of the SNR gain given by F can be found in Section V.

III. Experimental Setup

Fig. 2 shows the setup used to experimentally demonstrate the performance of the proposed method based on sub-bands processing. A low phase-noise, continuous-wave laser at $\lambda_0 =$ 1550 nm is connected to a Mach-Zehnder modulator (MZM) after passing a polarization controller (PC), to avoid polarization dependent losses. The MZM modulates the amplitude of the laser output according to a driving signal generated by an arbitrary waveform generator (AWG). The signal consists of rectangular chirped pulses at rate $R \cong 1.67$ kHz with temporal width $\tau_p = 200$ ns, total applied chirp $\delta\upsilon = 4$ GHz, and frequency shift $\widetilde{\upsilon_0} = 5$ GHz. The larger $\delta\upsilon$ with respect to usual values (~1 GHz) partially compensates the reduction in the maximum measurable $\Lambda(t)$ caused by sub-bands processing.

A semiconductor optical amplifier (SOA), with rise time of 1 ns and driven by a different (but synchronized) channel of the AWG, is used to increase the extinction ratio of the pulses. The optical spectrum of the modulated signal at the output of the SOA exhibits a central carrier at λ_0 and two symmetrical flat sidebands of same width $\delta\upsilon$, but opposite chirp rate, representing the spectrum of the linearly chirped pulses. By adjusting the MZM bias voltage, the amplitude of the carrier is reduced to match the peak amplitude of the sidebands, thus avoiding photodetector saturation due to strong DC components. To compensate the losses introduced mostly by the MZM, an erbium-doped fiber amplifier (EDFA) is inserted to boost the pulse power as much as possible but avoiding the onset of modulation instability. The amplified spontaneous emission noise (ASE) introduced by the EDFA is removed by a reflective fiber Bragg grating (FBG) filter, centered at λ_0, before launching the pulses into the fiber under test (FUT). The backscattering signal $E(t)$ generated by the FUT, whose spectrum still exhibits a double sideband modulation, is amplified by a second EDFA at the receiver front-end, followed by a narrow band (NB) optical filter. The bandwidth of the NB filter is tuned to suppress one of the chirped sidebands (with a high rejection of more than 30 dB) and the ASE. Note that while the choice of which sideband must be suppressed is irrelevant for the method, their chirp rate shows opposite sign thus affecting the sign of the results if not properly taken into account. Finally, a 12 GHz photodetector (PD), followed by an oscilloscope (OSC) triggered by the AWG is used to collect the received traces $I(t)$. Such traces are directly low-pass filtered by the OSC with a cut-off frequency $f_{LPF} = 9.5$ GHz to remove high-frequency noise. The decision of inserting the NB filter at the end of the setup was taken after observing that no gain reduction was induced in the first EDFA when both sidebands of the input pulse were being amplified. This solution allowed to minimize the total amount of ASE reaching the PD, thus improving the received signal quality.

The FUT consists of a standard single-mode optical fiber of length $L_{\text{FUT}} \cong 100$ m which incorporates aluminum alloy wires running in parallel to the fiber. The wires can be made accessible in various points where the FUT can be heated up

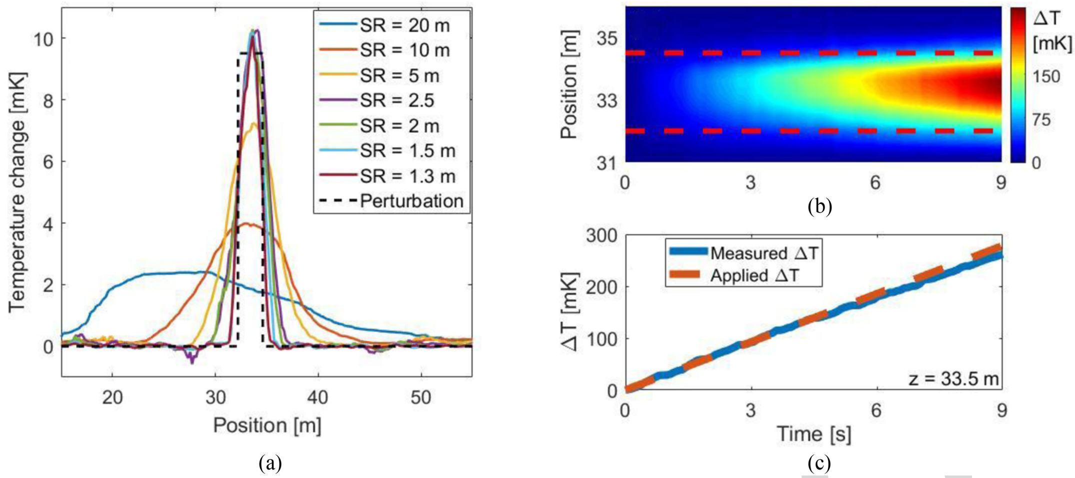

Fig. 3. (a) Temperature changes measured for different spatial resolutions with fixed overlap factor $F = 7$. The black dashed line represents the applied temperature change. (b) Temperature change measured over a temporal interval of 9 seconds (using $N = 10$ and $F = 7$). The red dashed lines identify the heated fiber section of length L_p. (c) Comparison between the measured temperature change magnitude with respect to the applied one.

through Joule effect by applying a voltage V_{FUT} between any two accessible points. The fiber-wire bundle is covered by a thick polymeric coating that allows for partial isolation from external perturbations, thus ideally securing a uniform and efficient temperature change. The temperature changes in the fiber as a function of the current are calibrated using standard CP phase sensitive reflectometry methods [18].

IV. Results

To experimentally demonstrate the spatial resolution improvement provided by sub-bands processing, a segment of the FUT of length $L_p = 2.5$ m, centered at position $z = 33.5$ m, has been heated up uniformly by applying a constant voltage $V_{\mathrm{FUT}} = 1.2$ V to the metallic wires attached to the FUT. The oscilloscope is set to acquire 2^{14} traces at a rate R, monitoring the perturbation acting on the fiber for about 9 seconds. To smooth down fast environmental changes that could reduce the quality of the correlation operation in (14), the traces collected every three consecutive acquisitions have been averaged, limiting the effective measurement rate to $R_{eff} \cong 550$ Hz. To secure a visible temperature change, two arbitrary traces separated by $\delta t = 0.24$ s, have been selected as $I_r(t)$ and $I_m(t)$, and the corresponding passband terms $I_{pb,r}(f)$ and $I_{pb,m}(f)$ have been extracted with a digital rectangular passband filter of width $\delta\upsilon$. Finally, the overlap factor has been set to $F = 7$ based on the optimization process described in Section V.

The proposed method has then been executed for different values of $N = [1,\ 2,\ 4,\ 8,\ 10,\ 13,\ 15]$,corresponding to spatial resolutions of $SR = [20,\ 10,\ 5,\ 2.5,\ 2,\ 1.5,\ 1.3]$ m and a total number of sub-bands $\tilde{N} = [1,\ 8,\ 22,\ 50,\ 64,\ 85,\ 99]$. Results are shown in Fig. 3(a), where we can see that, for the values of $N < 8$, corresponding to spatial resolutions larger than $L_p = 2.5$ m, the measured results show a hot-spot with distorted magnitude, spread over a section of the fiber proportional to the spatial resolution. In these cases, the longitudinal shift Λ of the local pattern of the backscattering trace $I^n_{pb,m}(t)$ occupies at most a fraction of the correlation window $\widetilde{\tau}_c$. Consequently, no improvement in the spatial resolution can be observed in Fig. 3(a) for $N < 8$, resulting in a temperature change profile having a distorted hot-spot. This effect can be especially observed for values of $N \leq 4$, when the amplitudes and the full-width at half-maximum of the measured hot-spot are visibly different from the applied temperature change (represented in the figure by the black dashed line). For values of $N \geq 8$, however, the size of the correlation window $\widetilde{\tau}_c$ is equal or shorter than the perturbed segment L_p. Hence, the temporal correlation in (14) correctly estimates the temperature-induced shifts with an improved spatial resolution. The results of the proposed method agree very well with the real applied temperature change. Observing the lines corresponding to $N \geq 8$ in Fig. 3(a), the effects of the increased spatial resolution can be verified by the sharper transitions in the temperature profile. Finally, Fig. 3(a) also shows that the procedure introduces only a minimal measurement SNR degradation, which can be verified by the small increase in the temperature profile oscillations out of the hot-spot location. This result confirms that the averaging operation between the traces $I^n_{\mathrm{xcorr}}(t)$ computed from overlapped sub-bands is an effective solution for compensating the SNR reduction.

It must be pointed out that the change in the input pulse indeed does not influence the high performance of the standard CP ϕ-OTDR setup such as the robustness to signal fading or the high sensitivity. This can be verified by tracking the temperature change of the fiber section around the position $z = 33.5$ m during the 9 s of acquisition. The results are shown in Fig. 3(b) and 3(c) where a linearly growing temperature change around the hot-spot can be observed over time without distortion or signal loss. For this measurement $N = 15$ has been chosen, thus securing a spatial resolution of $SR = 1.3$ m. As can be seen, the magnitude of the measured ΔT closely follows the applied perturbation and the position of the hot-spot is correctly identified, spread over a fiber section of length L_p.

To compare the advantages in monitoring long perturbations obtained by the sub-bands processing with respect to the original

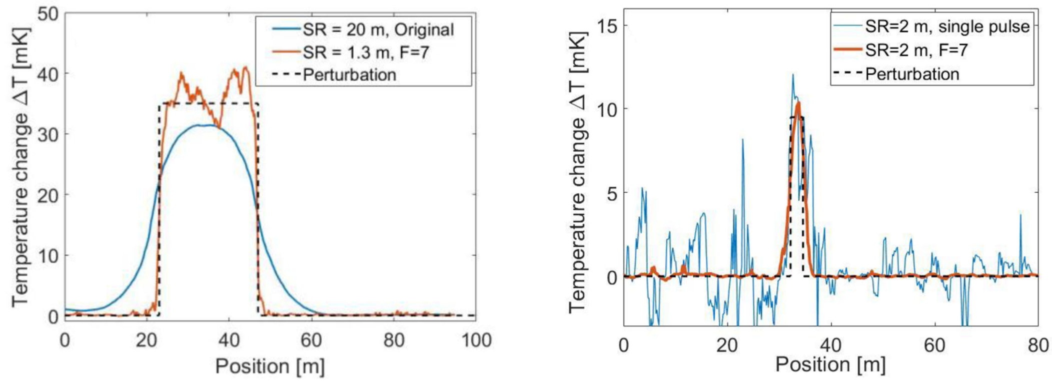

(a) (b)

Fig. 4. (a) Temperature change over 25 meters measured with the original chirped-pulse ϕ-OTDR method (SR $= 20$ meter) (blue line) and with the proposed high resolution method ($N = 10 \rightarrow SR = 2$ m, $F = 7$) (red line). (b) Comparison between the temperature profile measured with the original method and pulses of $\tau_p = 20$ ns, providing a spatial resolution $SR = 2$ m (blue line) and the temperature profile measured with the proposed high resolution method using pulses of $\tau_p = 200$ ns and setting $N = 10$, thus $SR = 2$ m and $F = 7$.

CP ϕ-OTDR, a temperature change has been induced on a fiber segment of length $L_p = 25$ m, centered around the position $z = 37$ m. As before, the temperature change has been generated through Joule heating of the metallic wires. However, to guarantee a visible perturbation over such a long fiber segment, the applied voltage has been raised up to $V_{\text{FUT}} = 8$ V. The traces have been first collected using the standard CP ϕ-OTDR setup, sending pulses of width $\tau_p = 200$ ns to provide a spatial resolution of $SR = 20$ m. After the acquisition, the power supply was turned off to let the fiber cool down to room temperature before turning it on again and measure with the proposed high-resolution setup. The measurement results obtained by both systems are shown in Fig. 4(a), where the blue line represents the temperature profile extracted with the standard setup, while the red one represents the high-resolution curve obtained through sub-bands processing. The reference and measurement traces have been separated by $\delta t = 0.24$ s in the two cases and a value of $N = 15$ has been chosen. As can be seen, the results obtained from both setups correctly identify the position and the magnitude of the perturbation but, as expected, the transients of the trace computed from the original CP ϕ-OTDR are much longer than the transients of the trace extracted by applying sub-bands processing. Moreover, the increased spatial resolution allows a more accurate evaluation of the perturbation affecting the fiber. In particular, the trace obtained by applying sub-bands processing highlights a non-uniform temperature profile along the perturbed fiber section, which is hidden in the standard setup by its low spatial resolution. The high-resolution trace exhibits a 2-fold reduction in the SNR evaluated outside the hot-spot region, compared to the trace measured with the original setup. Nevertheless, such an SNR reduction has only a negligible impact on the results quality.

A final demonstration of the performance improvement provided by the proposed method has been realized by comparing the measurements of a $L_p = 2.5$ m-long temperature change obtained by a standard CP ϕ-OTDR with a 2 m spatial resolution and the proposed method with the same resolution. For this, a standard CP ϕ-OTDR has been implemented using pulses of $\tau_p = 20$ ns and a total applied chirp of $\delta\upsilon = 0.4$ GHz. The proposed high-resolution CP ϕ-OTDR has been however implemented with much longer pulses of $\tau_p = 200$ ns, chirp of $\delta\upsilon = 4$ GHz, and $N = 10$ sub-bands, securing the same spatial resolution of $SR = 2$ m. As can be seen in Fig. 4(b), the temperature profile measured with sub-bands processing exhibits a much higher measurement quality compared to the one obtained by the standard setup. Indeed, while the measured temperature change matches the applied perturbation in both cases, the measurement with the standard setup shows high-amplitude spikes caused in the cross-correlation process due to the low measurement SNR. This way, result clearly demonstrates the significant improvement provided by the setup and sub-band processing proposed.

V. Overlap Factor Optimization

Section II described the technique proposed in this paper based on the extraction of overlapped sub-bands from the spectrum $I_{pb}(f)$, followed by an averaging process to mitigate the consequent SNR reduction. To extract overlapped sub-bands, the central frequency of the applied digital passband filter is shifted in steps of $\delta W = \Delta W/F$, where F is an integer number called overlap factor. Using then a factor $F > 1$ results in $\tilde{N} = F(N-1)+1 > N$ overlapped sub-bands. Assuming the noise affecting $I_{pb}(f)$ to be white, for $F = 1$ the N independent sub-bands will all have uncorrelated noise. This can secure the maximum efficiency in the averaging process described in (15), to reduce the error in the estimation of the shifts $\Lambda(\text{t})$. Using large values of F, a high number of windows can be exploited for averaging; however, the noise affecting overlapped sub-bands becomes progressively more correlated and the efficiency of the averaging process is reduced. A high value of F will not then proving any benefit. Nevertheless, low values of F still guarantee significant SNR mitigation gains. This is clearly represented in Fig. 5(a), which shows the retrieved temperature profile over an unperturbed fiber section (i.e., the impact of the system noise) for different overlap factors F. Fig. 5(b) shows the temperature

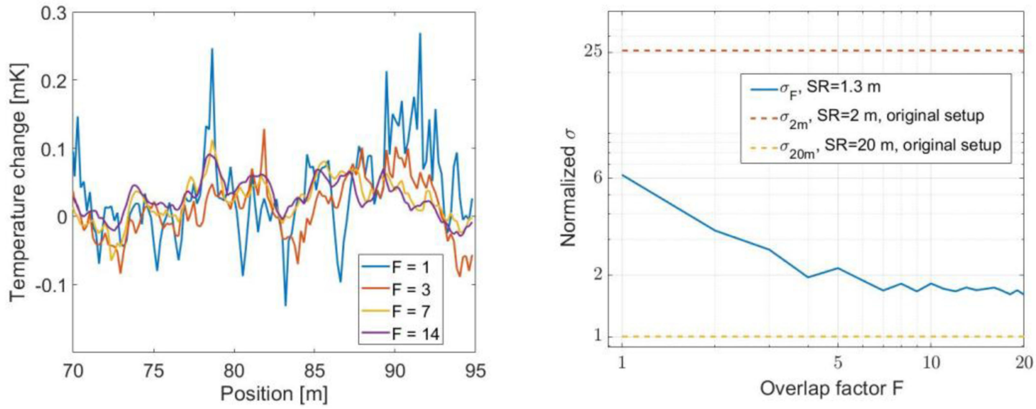

(a) (b)

Fig. 5. (a) Comparison between the unperturbed sections of the fiber measured for different values of F; (b) Normalized standard deviation σ for different values of F compared with the normalized standard deviations of the original setup with different spatial resolutions.

standard deviation measured over fiber locations out of the applied hot-spot, showing a strong reduction of the temperature noise when increasing F from 1 to 7. The improvement is however significantly reduced when F is increased to 14. The total chirp $\delta\upsilon$ applied to the pulse affects the overlap factor, since for a given F a larger chirp implies a larger bandwidth of the K sub-bands and a lower noise correlation. To achieve the highest SNR mitigation gain, the optimal value of F must then be identified every time the pulse parameters are changed. However, often the value of $F = 7$ can be considered a default considering that the complexity of the algorithm increases for increasing values of F and that the normalized standard deviation does not change significantly beyond that value.

The easiest way to identify the optimum value of the overlap factor consists in computing the noise standard deviation σ of the retrieved temperature profile as a function of F. The data represented in Fig. 4(a) are used to perform this analysis, in order to allow a comparison of the σ achieved with our technique with respect to the original setup. For our setup, the overlap factor F has been varied from 1 to 20 and the σ_F have been computed in the short unperturbed fiber section $S = [70,\ 95]$ m since, as can be seen in Fig. 5(a), the noise evolves over lengths much shorter than the spatial resolution and the high spatial sampling guarantees a sufficiently accurate estimation. For the original setup, where the input pulse width has been set to $\tau_p = 200$ ns to provide a $SR = 20\ m$, the standard deviation $\sigma_{20\mathrm{m}}$ is computed over the same section S. The σ_F have been normalized then to $\sigma_{20\mathrm{m}}$ to highlight the SNR reduction introduced by our technique with respect to the original system. As can be seen in Fig. 5(b), the σ_F show a decreasing behavior for increasing values of F, which corresponds to a progressively stronger mitigation of the SNR reduction. The curve saturates at a mean value of 1.77 after $F = 7$, proving that the proposed method may achieve a significant SR improvement at the cost of a SNR reduction lower than a factor 2 with respect to the original setup. Since an overlap factor greater than $F = 7$ does not provide any further improvement, it can be considered as the optimal one for the chosen parameters. For the sake of comparison, the normalized standard variation of the noise $\sigma_{2\mathrm{m}}$ of the original setup when a pulse of width $\tau_p = 20$ ns, $SR = 2$ m, is used (data represented in Fig. 4(b)) is added to Fig. 5(b). As can be seen, in such a case our technique guarantees better performance even without using overlapped sub-bands.

VI. Conclusion

In this paper, a method to improve the spatial resolution of CP ϕ-OTDR systems based on sub-bands processing has been proposed and experimentally demonstrated. The division of the fiber response to the chirped pulse into spectral sub-bands, and the consequent processing, allows to convert a measurement performed with a long pulse (and hence a low spatial resolution), in a measurement with high spatial resolution at the cost of a slightly reduced SNR (less than a factor 2 in our demonstration). The reduced pulse width caused by the sub-band processing, proportionally limits the maximum shot-to-shot measurable temperature or strain gradient. However, for the trigger rates and chirp bandwidths used in this work this range reduction still allow measuring the vast majority of physical processes of interest (e.g., intrusions, small seismic features, etc.). Note that in all cases, the actual measurement range can exceed substantially that one allowed by the chirp bandwidth, simply by using temporally adjacent traces and keeping track of the previous measurements [24]. Note also that to avoid distortions in the linear chirp generated by the MZM, the intensity of the driving signal generated by the AWG has to be reduced, limiting the magnitude of the generated chirped sidebands and consequently the maximum measurement range. By implementing more precise techniques to realize the sidebands or by finding a different way to add the carrier to the input pulse, without increasing the phase noise, such limitation can be further relaxed.

References

[1] T. M. Daley, B. M. Freifeld, J. Ajo-Franklin, and S. Dou, "Field testing of fiber-optic distributed acoustic sensing (DAS) for subsurface seismic monitoring," *Leading Edge*, vol. 32, no. 6, pp. 699–706, Jun. 2013.

[2] L. Schenato *et al.*, "Distributed optical fibre sensing for early detection of shallow landslides triggering," *Sci. Rep.*, vol. 7, no. 1, Oct. 2017, Art. no. 14686.

[3] H. F. Martins, S. Martin-Lopez, P. Corredera, J. D. Ania-Castañon, O. Frazão, and M. Gonzalez-Herraez, "Distributed vibration sensing over 125 km with enhanced SNR using phi-OTDR over a urfl cavity," *J. Lightw. Technol.*, vol. 33, no. 12, pp. 2628–2632, Jun. 2015.

[4] L. Marcon, A. Galtarossa, and L. Palmieri, "High-frequency high-resolution distributed acoustic sensing by optical frequency domain reflectometry," *Opt. Express*, vol. 27, no. 10, May 2019, Art. no. 13923.

[5] J. C. Juarez, E. W. Maier, K. N. Choi, and H. F. Taylor, "Distributed fiber-optic intrusion sensor system," *J. Light. Technol.*, vol. 23, no. 6, Jun. 2005, Art. no. 2081.

[6] H. F. Martins, S. Martin-Lopez, P. Corredera, P. Salgado, O. Frazão, and M. González-Herráez, "Modulation instability-induced fading in phase-sensitive optical time-domain reflectometry," *Opt. Lett.*,vol. 38, no. 6, pp. 872–874, Mar. 2013.

[7] Z. He, Q. Liu, X. Fan, D. Chen, S. Wang, and G. Yang, "Fiber-optic distributed acoustic sensors (DAS) and applications in railway perimeter security," *Proc. SPIE*, vol. 10821, Oct. 2018, Art. no. 1082102.

[8] L. Costa *et al.*, "Fast and direct measurement of the linear birefringence profile in standard single-mode optical fibers," *Opt. Lett.*, vol. 45, no. 3, pp. 623–626, Jan. 2020.

[9] P. Healey, "Fading in heterodyne OTDR," *Electron. Lett.*, vol. 20, no. 1, pp. 30–32, Jan. 1984.

[10] T. Zhu, Q. He, X. Xiao, and X. Bao, "Modulated pulses based distributed vibration sensing with high frequency response and spatial resolution," *Opt. Express*, vol. 21, no. 3, pp. 2953–2963, Feb. 2013.

[11] Y. Muanenda, C. J. Oton, S. Faralli, and F. D. Pasquale, "A cost-effective distributed acoustic sensor using a commercial off-the-shelf DFB laser and direct detection ϕ-OTDR," *IEEE Photon. J.*, vol. 8, no. 1, pp. 1–10, Feb. 2016.

[12] M. A. Soto, J. A. Ramírez, and L. Thévenaz, "Intensifying the response of distributed optical fibre sensors using 2D and 3D image restoration," *Nat. Commun.*, vol. 7, Mar. 2016, Art. no. 10870.

[13] J. Pastor-Graells, H. F. Martins, A. Garcia-Ruiz, S. Martin-Lopez, and M. Gonzalez-Herraez, "Single-shot distributed temperature and strain tracking using direct detection phase-sensitive OTDR with chirped pulses," *Opt. Express*, vol. 24, no. 12, Jun. 2016, Art. no. 13121.

[14] B. Lu *et al.*, "High spatial resolution phase-sensitive optical time domain reflectometer with a frequency-swept pulse," *Opt. Lett.*, vol. 42, no. 3, pp. 391–394, Feb. 2017.

[15] M. R. Fernández-Ruiz, J. Pastor-Graells, H. F. Martins, A. Garcia-Ruiz, S. Martin-Lopez, and M. Gonzalez-Herraez, "Laser phase-noise cancellation in chirped-pulse distributed acoustic sensors," *J. Light. Technol.*, vol. 36, no. 4, pp. 979–985, Feb. 2018.

[16] D. Chen, Q. Liu, X. Fan, and Z. He, "Distributed fiber-optic acoustic sensor with enhanced response bandwidth and high signal-to-noise ratio," *J. Light. Technol.*, vol. 35, no. 10, pp. 2037–2043, May 2017.

[17] D. Chen, Q. Liu, Y. Wang, H. Li, and Z. He, "Fiber-optic distributed acoustic sensor based on a chirped pulse and a non-matched filter," *Opt. Express*, vol. 27, no. 20, Sep. 2019, Art. no. 29415.

[18] J. J. Mompó, L. Shiloh, N. Arbel, N. Levanon, A. Loayssa, and A. Eyal, "Distributed dynamic strain sensing via perfect periodic coherent codes and a polarization diversity receiver," *J. Light. Technol.*, vol. 37, no. 18, pp. 4597–4602, Sep. 2019.

[19] S. Liehr, S. Münzenberger, and K. Krebber, "Wavelength-scanning coherent OTDR for dynamic high strain resolution sensing," *Opt. Express*, vol. 26, no. 8, pp. 10573–10588, Apr. 2018.

[20] 1. D. Chen, Q. Liu, and Z. He, "High-fidelity distributed fiber-optic acoustic sensor with fading noise suppressed and sub-meter spatial resolution," *Opt. Express*, vol. 26, no. 13, pp. 16138–16146, Jun. 2018.

[21] L. Marcon, M. A. Soto, M. Soriano-Amat, L. Costa, H. F. Martins, L. Palmieri, and M. Gonzalez-Herraez, "Boosting the spatial resolution in chirped pulse ϕ-OTDR using sub-band processing," in *Proc. 17h Eur. Workshop Opt. Fibre Sensors*, 2019, vol. 11199, Art. no. 111991W.

[22] J. S. Sirkis and H. W. Haslach, "Interferometric stain measurement by arbitrarily configured surface-mounted, optical fibers," *J. Light. Technol.*, vol. 8, no. 10, pp. 1497–1503, Oct. 1990.

[23] Y. Koyamada, M. Imahama, K. Kubota, and K. Hogari, "Fiber-optic distributed strain and temperature sensing with very high measurand resolution over long range using coherent OTDR," *J. Light. Technol.*, vol. 27, no. 9, pp. 1142–1146, May 2009.

[24] H. D. Bhatta *et al.*, "Dynamic measurements of 1000 microstrains using chirped-pulse phase-sensitive optical time-domain reflectometry," *J. Light. Technol.*, vol. 37, no. 18, pp. 4888–4895, Sep. 2019.

GENERAL INSTRUCTIONS

- **Authors: When accessing and uploading your corrections at the Author Gateway, please note we cannot accept new source files as corrections for your article. Do not send new Latex, Word, or PDF files, as we cannot simply "overwrite" your article. Please submit your corrections as an annotated PDF or as clearly written list of corrections, with location in article, using line numbers provided on your proof. You can also upload revised graphics to the Gateway.**
- **Authors: Please note that once you click "approve with no changes," the proofing process is now complete and your article will be sent for final publication and printing. Once your article is posted on Xplore, it is considered final and the article of record. No further changes will be allowed at this point so please ensure scrutiny of your final proof.**
- **Authors: Unless invited or otherwise informed, overlength page charges of $260 per page are mandatory for each page in excess of seven printed pages and are required for publication. If you have any questions regarding overlength page charges, need an invoice, or have any other billing questions, please contact reprints@ieee.org as they handle these billing requests.**

QUERY

Q1. Author: Please confirm or add details for any funding or financial support for the research of this article.

High-Resolution Chirped-Pulse ϕ-OTDR by Means of Sub-Bands Processing

Leonardo Marcon, Marcelo A. Soto, Miguel Soriano-Amat, Luis Costa, Maria R. Fernandez-Ruiz, Hugo F. Martins, Luca Palmieri, and Miguel Gonzalez-Herraez

***Abstract*—Conventional chirped-pulse (CP) phase-sensitive optical time-domain reflectometry (CP ϕ-OTDR) allows the interrogation of tens of kilometers of optical fiber with high accuracies of millikelvin or nanostrain. With respect to standard coherent-detection ϕ-OTDR, it shows increased robustness to coherent fading and allows a linear and quantitative monitoring of the perturbations acting on the fiber. Its spatial resolution, however, remains a critical parameter and new techniques allowing its improvement without reducing significantly other performances (or increasing the setup complexity) are constantly being researched. In this paper, we propose a method to improve the spatial resolution of CP ϕ-OTDR without reducing the input pulse width, by means of sub-bands processing. The method is based on adding an optical carrier to the input pulse. Using digital filtering, the spectrum of the fiber backscatter can be split into multiple sub-bands. Each of these sub-bands corresponds to the fiber response generated by a short optical pulse, chirped over a smaller frequency range. This way each sub-band results in ϕ-OTDR measurements with high spatial resolution, but with a reduced SNR. A dedicated post-processing methodology is proposed to mitigate the SNR reduction obtained from each sub-band, while securing high-resolution measurements of the perturbations acting on the fiber. Experimental results demonstrate the possibility of achieving CP ϕ-OTDR measurements with a 15-fold spatial resolution improvement over the conventional CP analysis, at the expense of an SNR reduction lower than a factor 2.**

***Index Terms*—Digital signal processing, phase-sensitive optical time-domain reflectometry, Rayleigh scattering.**

Manuscript received October 31, 2019; revised January 16, 2020 and March 4, 2020; accepted March 14, 2020. Date of publication; date of current version. This work was supported in part by Project FINESSE MSCA-ITN-ETN-722509, in part by the DOMINO Water JPI project under the WaterWorks2014 cofounded call by EC Horizon 2020, in part by ERANET Cofund Water Works 2014 call, Spanish MINECO and Italian MIUR, in part by Comunidad de Madrid and FEDER Program under Grant SINFOTON2-CM: P2018/NMT-4326, and in part by MINECO under Project RTI2018-097957-B-C31. The work of Leonardo Marcon was supported by Fondazione Ing. Aldo Gini. Marcelo A. Soto was supported in part by AC3E ANID-Basal Project FB0008 and in part by "Becas Iberoamérica Santander Universidades Convocatoria 2018" (research stay at Universidad de Alcalá, Spain). The work of Maria R. Fernandez-Ruiz and Hugo F. Martins were supported by the Spanish Ministerio de Ciencia, Innovación y Universidades (CIENCIA) under Contracts FJCI-2016-27881 and IJCI-2017-33856. (*Corresponding author: Leonardo Marcon.*)

Leonardo Marcon and Luca Palmieri are with the Department of Information Engineering, University of Padova, 35131 Padova, Italy (e-mail: leonardo.marcon.1@phd.unipd.it; luca.palmieri@dei.unipd.it).

Marcelo A. Soto is with the Department of Electronic Engineering, Universidad Técnica Federico Santa María, 2390123 Valparaíso, Chile (e-mail: marcelo.sotoh@usm.cl).

Miguel Soriano-Amat, Luis Costa, Maria R. Fernandez-Ruiz, and Miguel Gonzalez-Herraez are with the Departamento de Electronica, Universidad de Alcalá, Edificio Politécnico, 28871 Madrid, Spain (e-mail: miguel.soriano@uah.es; ldpcosta@gmail.com; rosario.fernandezr@uah.es; miguel.gonzalezh@uah.es).

Hugo F. Martins is with the Instituto de Óptica "Daza de Valdés", IO-CSIC, 28006 Madrid, Spain (e-mail: h.fidalgo@uah.es).

Color versions of one or more of the figures in this article are available online at http://ieeexplore.ieee.org.

Digital Object Identifier 10.1109/JLT.2020.2981741

I. Introduction

Distributed acoustic sensors (DAS) based on Rayleigh backscattering have become fundamental elements for safety applications [1], [2], particularly in harsh environments. The possibility of performing the analysis either in time-domain or frequency-domain guarantees flexible performance between coarse long-range [3] and accurate short-range [4] monitoring.

Phase-sensitive optical time-domain reflectometry (ϕ-OTDR) [5] is one of the most common DAS configurations due to its good performance and reduced cost. It requires a pulsed coherent light source that allows the interrogation of tens of kilometers of optical fiber with an acoustic bandwidth of few kilohertz and a spatial resolution proportional to the launched pulse width. The amplitude and temporal width of the optical pulses determine the amount of power backscattered from the fiber so, to guarantee a sufficient signal to noise ratio (SNR) in the measurement, either the amplitude must be increased, or long pulses must be used. The onset of nonlinear phenomena like modulation instability [6] imposes strong limits to the maximum pulse amplitude allowed at the fiber input. This way, the use of long pulses, which may force spatial resolutions in the order of tens of meters, becomes unavoidable to obtain DAS measurements with high SNR. Therefore, the use of ϕ-OTDR is limited to those DAS applications where an accurate spatial monitoring is not necessary [7], [8].

In recent years, many efforts have been made to reduce the drawbacks of ϕ-OTDR setups, specifically coherent fading [9] and its nonlinear response to the perturbations acting on the fiber [10]–[12]. By introducing a linear chirp into the input pulse, such drawbacks can be strongly mitigated [13], [14]. The CP ϕ-OTDR setup guarantees a linear measurement of the perturbations, while securing an increased robustness to coherent fading and high temperature and strain resolutions (e.g., millikelvin and nanostrain levels) [15]. The spatial resolution, however, remains limited by the pulse width. Possible solutions for such issue can be found modifying the CP ϕ-OTDR setup into a TGD-OFDR [16], [17], or by using optical pulse coding [18] or wavelength-scanning coherent OTDR [19]. With these techniques sub-meter spatial resolutions have been achieved over long distances, at the cost of a higher complexity and cost [20].

In this paper, we propose a method based on sub-bands processing to improve the spatial resolution of the CP ϕ-OTDR, with minimal changes to the original setup and without reducing the width of the optical pulse. An optical carrier at a specific frequency is added to the interrogating pulse, allowing the extraction of the fiber response to the chirped pulse from the signal received at an intermediate frequency. By using digital filters, the spectrum of the fiber response is divided into multiple sub-bands, eventually overlapped, being conceptually analogous to the spectra of the fiber response generated by multiple slightly delayed short pulses. The analysis of any one of these sub-bands guarantees ϕ-OTDR traces characterized by high resolution but reduced SNR and shot-to-shot maximum measurable strain-temperature change. By performing an averaging operation during the analysis of the sub-bands, a mitigation of the SNR reduction can be achieved.

In this manuscript, starting from the description of the standard CP ϕ-OTDR setup and extending our preliminary results in [21], we derive a mathematical model of the backscattered response generated by an interrogation signal containing a linearly chirped pulse and an added optical carrier at a different frequency. We then describe the sub-bands processing, analyzing in detail the averaging operation used to mitigate the expectable SNR reduction obtained with this method. In addition, we propose an experimental setup to demonstrate the spatial resolution enhancement guaranteed by the sub-bands processing and we compare the results with those obtained from a standard CP ϕ-OTDR. By accepting a modest reduction of the measurement SNR and of the shot-to-shot maximum measurable strain-temperature change, experimental results demonstrate a 15-fold improvement of the spatial resolution. Finally, we discuss the advantages of overlapped sub-bands to increase the number of terms in the averaging operation and we optimize the process. To have a higher control over the fiber perturbed sections and to focus on the working principle of the propose method we used slow temperature changes as perturbations. No variation of the sensors dynamic capability should occur if a sufficient processing power is available.

II. Theoretical Model

In a standard CP ϕ-OTDR [18] the input pulse $P_{\text{std}}(t, z)$ can be defined as:

$$P_{\text{std}}\left(t, z\right) = E_0 \text{rect}\left[\frac{t - \beta_1\left(z\right)}{\tau_p}\right] P_{cp}\left(t, z\right) \tag{1}$$

where E_0 is the pulse field amplitude, $\beta_1(z) = \int_0^z n_g(z)dz/c$ is the propagation delay, τ_p is the pulse width and:

$$P_{cp}\left(t, z\right) = e^{j2\pi(\upsilon_0 + \delta\upsilon/\tau_p[t - \beta_1(z)])(t - \beta_1(z))} \tag{2}$$

is the linearly chirped term with total applied chirp $\delta\upsilon$.

As $P_{\text{std}}(t, z)$ propagates along the fiber, it generates a Rayleigh backscattering signal that represents the fiber response to the chirped pulse. This response can be described as the convolution $*$ of the input pulse with the fiber Rayleigh backscattering profile function $r(z)$:

$$E_{\text{std}}\left(t\right) = P_{\text{std}}\left(t, z\right) * r\left(z\right). \tag{3}$$

Upon detection $E_{\text{std}}(t)$ is converted from the optical to the electrical domain, resulting in a photocurrent described as:

$$I_{\text{std}}\left(t\right) = E_{\text{std}}\left(t\right) {E_{\text{std}}}^{cc}\left(t\right) \tag{4}$$

where cc stands for complex conjugation and each time instant t can be associated with a fiber position z by $t = 2nz/c$.

When a perturbation acts on a position z_0 of the fiber, it induces a change Δn in the local refractive index [22]. Using a chirped pulse ϕ-OTDR to interrogate the fiber, in correspondence to the position z_0, Δn generates a linearly proportional longitudinal shift Λ of the local pattern of $I_{\text{std}}(t)$:

$$\frac{\Delta n}{n} = -\left(\frac{1}{\upsilon_0}\right)\left(\frac{\delta\upsilon}{\tau_p}\right)\Lambda, \tag{5}$$

which can be immediately translated into temperature or strain changes (e.g., ΔT or $\Delta\varepsilon$, respectively) through the relations [23]:

$$\left(\frac{1}{\upsilon_0}\right)\left(\frac{\delta\upsilon}{\tau_p}\right)\Lambda = 0.78 \cdot \Delta\varepsilon,$$
$$\left(\frac{1}{\upsilon_0}\right)\left(\frac{\delta\upsilon}{\tau_p}\right)\Lambda = \left(6.92 \cdot 10^{-6}\right) \cdot \Delta T. \tag{6}$$

By monitoring the longitudinal shifts in the pattern of $I_{\text{std}}(t)$ along the whole fiber, the local perturbations affecting the sensing fiber can be completely characterized.

A standard CP ϕ-OTDR interrogates the fiber with two identical pulses. Those pulses generate two traces, called reference $I_{std,r}(t)$ and measurement $I_{std,m}(t)$, obtained with a time difference δt. The shifts $\Lambda(t)$ over the temporal trace are calculated by a temporal cross-correlation operation $\star$ over a moving window along $I_{std,r}(t)$ and $I_{std,m}(t)$, defined by a correlation time $\tau_c \cong \tau_p$, which defines the spatial resolution:

$$I_{\text{xcorr}}\left(t\right) = I_{std,r}\left(t - \tau_c, t + \tau_c\right) \star I_{std,m}\left(t - \tau_c, t + \tau_c\right), \tag{7}$$

$$\Lambda\left(t\right) = \text{argmax}\left(I_{\text{xcorr}}\left(t\right)\right). \tag{8}$$

Using (6), $\Lambda(t)$ is converted to the corresponding ΔT or $\Delta\varepsilon$.

Any improvement in the spatial resolution of the CP ϕ-OTDR is hindered by the direct detection process in (4), which scrambles the spectral information contained in the fiber response to the chirped pulse $E_{\text{std}}(t)$. The easiest way to solve this issue and extract $E_{\text{std}}(t)$ consists in implementing a coherent receiver, but the necessity of a highly coherent laser, as well as the increased phase noise induced by the local oscillator and the need of polarization diversity in the receiver makes this alternative unappealing. To measure $E_{\text{std}}(t)$, we propose to modify the CP ϕ-OTDR interrogating signal in (1) by adding to the input pulse a separate optical carrier, so that:

$$P\left(t, z\right) = E_0 \text{rect}\left[\frac{t - \beta_1\left(z\right)}{\tau_p}\right]\left(P_{oc}\left(t, z\right) + P_{cp}\left(t, z\right)\right), \tag{9}$$

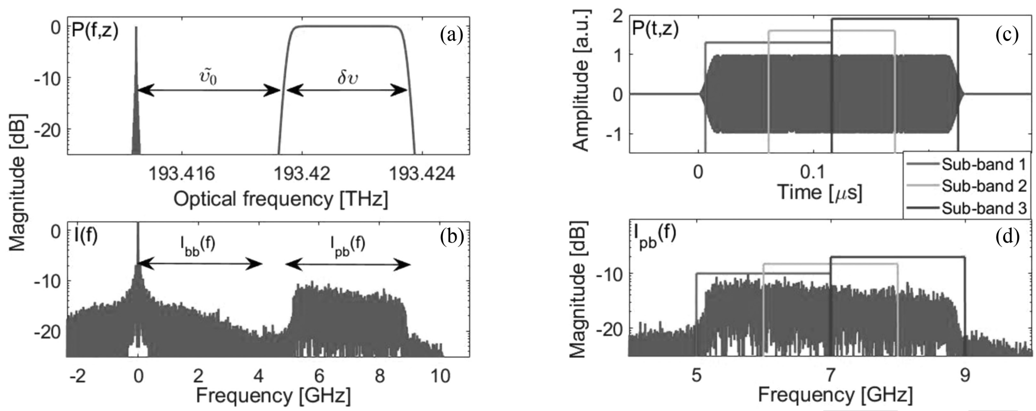

Fig. 1. (a) Optical spectrum of the input pulse $P(t,z)$, with $\delta\upsilon = 4$ GHz and $\widetilde{\upsilon_0} = 5$ GHz. (b) Electrical spectrum of the received backscattering signal $I(t)$ with highlighted baseband and passband terms. (c) Input optical pulse $P(t,z)$ with three overlapping sub-windows ($N = 2,\ F = 2$). (d) Pass-band term $I_{pb}(f)$ divided into three sub-bands. Each sub-band corresponds to the Rayleigh spectral response associated to one of the sub-windows in (c).

where:

$$P_{oc}(t,z) = e^{j2\pi(\upsilon_0-\widetilde{\upsilon_0})(t-\beta_1(z))},$$
$$P_{cp}(t,z) = e^{j2\pi(\upsilon_0+\delta\upsilon/\tau_p[t-\beta_1(z)])(t-\beta_1(z))}, \qquad (10)$$

are respectively the optical carrier at an optical frequency $\upsilon_0 - \widetilde{\upsilon_0}$, and the chirped pulse described in (2). Note that $P_{oc}(t,z)$ and $P_{cp}(t,z)$ have different central optical frequencies, as exemplified in Fig. 1(a). Due to the linearity of convolution, the propagation of the modified pulse $P(t,z)$ along the fiber can be modelled as the generation of two backscattering components:

$$E(t) = P(t,z) * r(z) = E_{oc}(t) + E_{cp}(t), \qquad (11)$$

and upon reception, the electrical signal becomes:

$$I(t) = E(t)\,E^*(t) = I_{bb}(t) + I_{pb}(t), \qquad (12)$$

where $I_{bb}(t) = |E_{oc}(t)|^2 + |E_{cp}(t)|^2$ and, by calling $\Re(\cdot)$ the real part operator, $I_{pb}(t) = 2\Re(E_{oc}(t)E_{cp}{}^*(t))$. As can be seen in Fig. 1(b), the spectrum $I_{bb}(f) = \mathcal{F}(I_{bb}(t))$ is a baseband, triangularly shaped term and, if we neglect the contribution of the added carrier, it corresponds to the spectrum of the signal received by the standard CP ϕ-OTDR in (4). The spectrum $I_{pb}(f) = \mathcal{F}(I_{pb}(t))$ is passband instead and, considering the optical carrier as a pure spectral line, it represents the fiber response to the chirped pulse $E_{cp}(t)$. Given that the spectral width of $I_{bb}(f)$ is twice the spectral width of $P_{cp}(t,z)$, the frequency shift in (9) must be at least $\widetilde{\upsilon_0} > \delta\upsilon$ to avoid overlaps with the spectrum of $I_{pb}(f)$. In the following analysis we will focus on $I_{pb}(f)$ which, assuming that the condition for the frequency shift $\widetilde{\upsilon_0}$ is satisfied, can be extracted from the received signal $I(f)$ by proper digital filtering. Due to the linear chirp applied to $P_{cp}(t,z)$, any sub-window of the input pulse in (9) generates a specific sub-band in $I_{pb}(f)$, as can be seen in Fig. 1(c) and 1(d). The spectrum of each sub-band corresponds to the spectrum generated when interrogating the fiber with a single short pulse, thus its analysis guarantees a sharp spatial resolution (i.e., improved with respect to the use of the entire chirped pulse), but at the cost of a reduced SNR and maximum shot-to-shot $\Lambda(t)$. The SNR reduction can be mitigated by exploiting the redundant information contained in the sub-bands: since they are extracted from the same pulse they correspond to simultaneous measurements of the same perturbations. The receiver noise affecting the different high-resolution ϕ-OTDR sections is uncorrelated, thus an averaging operation, accounting for the temporal shifts introduced during the sub-bands' extraction, can allow a strong SNR reduction mitigation while securing high spatial resolution measurements.

The measurement approach of the proposed scheme starts like the conventional CP ϕ-OTDR, by acquiring the reference $I_r(t)$ and measurement $I_m(t)$ traces at time instants separated by δt. Then, the corresponding bandpass components $I_{pb,r}(f)$ and $I_{pb,\ m}(f)$ are extracted using a digital band-pass filter of width $\delta\upsilon$. As mentioned above, the spatial resolution of an OTDR setup is proportional to the interrogating pulse width. Therefore, to improve the resolution by a factor N, it is necessary to split $I_{pb,r}(f)$ and $I_{pb,\ m}(f)$ into N independent sub-bands $I^n_{pb,r}(f)$, $I^n_{pb,m}(f),\ n = 1,\ldots N$ of width $\Delta W = \delta\upsilon/N$ and to adapt the correlation time accordingly $\widetilde{\tau_c} = \tau_p/N$. Each pair (reference and measurement) of sub-bands is converted to time-domain after synchronizing the filtering induced time shift:

$$I^n_{pb,r}(t) = \mathcal{F}^{-1}\left\{e^{-j2\pi f(n-1)\widetilde{\tau_c}} I^n_{pb,r}(f)\right\},$$
$$I^n_{pb,m}(t) = \mathcal{F}^{-1}\left\{e^{-j2\pi f(n-1)\widetilde{\tau_c}} I^n_{pb,m}(f)\right\}. \qquad (13)$$

The cross-correlation traces obtained from (7) are computed for each corresponding pair of $I^n_{pb,r}(t)$ and $I^n_{pb,m}(t)$, using the reduced correlation time $\widetilde{\tau_c}$ so that:

$$I^n_{\mathrm{xcorr}}(t) = I^n_{pb,r}(t-\widetilde{\tau_c}, t+\widetilde{\tau_c}) \star I^n_{pb,m}(t-\widetilde{\tau_c}, t+\widetilde{\tau_c}) \quad (14)$$

and then averaged into a single one:

$$I_{\mathrm{xcorr}}(t) = \frac{1}{N}\sum_{n=1}^{N} I^n_{\mathrm{xcorr}}(t). \qquad (15)$$

The shifts $\Lambda(t)$ along the fiber are then extracted using the operation in (8) and converted to the corresponding temperature or strain change through the equations in (6).

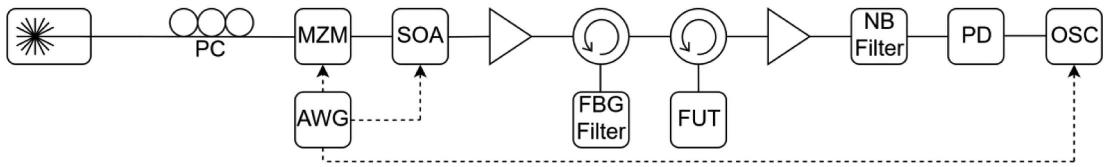

Fig. 2. Schematic representation of the experimental setup (the acronyms are explained in the text).

Averaging the cross-correlation traces $I^n_{\mathrm{xcorr}}(t)$ as described in (15) is key for the operation of the proposed method to increase the spatial resolution of the CP ϕ-OTDR, as it mitigates the critical SNR reduction induced when dividing $I_{pb}(f)$ into sub-bands. The extraction of $\Lambda(t)$ in (8) works properly only when the central correlation peak is the highest, but if two traces with low SNR are used in (14), noise-induced side peaks at random lags may exhibit higher magnitudes. In such cases, $\Lambda(t)$ extracted from (8) is an outlier value and does not represent the perturbation affecting the fiber. Even after averaging all the shifts extracted from the N different correlation traces, the results will only be comparable (in terms of SNR) to the ones obtained using directly a single short pulse, thus generally with an SNR being too low to be useful. However, since the noise-induced side peaks in (1) appear at different lags for different cross-correlation traces, their amplitude can be significantly dampened by averaging $I^n_{\mathrm{xcorr}}(t)$, allowing a correct extraction of the central correlation peak shift. It is not possible to use an arbitrary high value of N since a too low SNR and correlation time will generate chaotic results with no recoverable information. Since each sub-window corresponds to a shorter pulse, also the maximum $\Lambda(t)$ measurable shot-to-shot will be reduced. However, using standard parameters, such value will still be enough to monitor the vast majority of usual perturbations. The slight unevenness (<5 dB) of the band $I_{pb}(f)$ visible in Fig. 1(d) does not influence the quality of the results since the method is based on temporal cross-correlations. Such distortion will only impact slightly the amplitude of the correlation traces, but not the information of the temperature-strain perturbations contained in the temporal shift of the correlation peak.

So far, the description of the method has been based on the use of non-overlapping independent sub-windows, exhibiting uncorrelated noise that guarantees an efficient noise reduction by the averaging operation in (15). Such efficiency is reduced if partially overlapped sub-windows are used. This is because of the increased noise correlation; however, a larger number of terms available for averaging can compensate this effect, securing a good mitigation of the SNR reduction. Defining the shift between the central frequency of consecutive sub-bands as $\delta W = \Delta W / F$, with F being an integer number called overlap factor, $\tilde{N} = F(N-1)+1 > N$ partially overlapped sub-bands can be extracted setting $F > 1$. Since the noise of progressively overlapped sub-bands exhibits a growing correlation, the improvement provided by higher F value will saturate. The analysis of the SNR gain given by F can be found in Section V.

III. Experimental Setup

Fig. 2 shows the setup used to experimentally demonstrate the performance of the proposed method based on sub-bands processing. A low phase-noise, continuous-wave laser at $\lambda_0 =$ 1550 nm is connected to a Mach-Zehnder modulator (MZM) after passing a polarization controller (PC), to avoid polarization dependent losses. The MZM modulates the amplitude of the laser output according to a driving signal generated by an arbitrary waveform generator (AWG). The signal consists of rectangular chirped pulses at rate $R \cong 1.67$ kHz with temporal width $\tau_p = 200$ ns, total applied chirp $\delta\upsilon = 4$ GHz, and frequency shift $\widetilde{\upsilon_0} = 5$ GHz. The larger $\delta\upsilon$ with respect to usual values (~1 GHz) partially compensates the reduction in the maximum measurable $\Lambda(t)$ caused by sub-bands processing.

A semiconductor optical amplifier (SOA), with rise time of 1 ns and driven by a different (but synchronized) channel of the AWG, is used to increase the extinction ratio of the pulses. The optical spectrum of the modulated signal at the output of the SOA exhibits a central carrier at λ_0 and two symmetrical flat sidebands of same width $\delta\upsilon$, but opposite chirp rate, representing the spectrum of the linearly chirped pulses. By adjusting the MZM bias voltage, the amplitude of the carrier is reduced to match the peak amplitude of the sidebands, thus avoiding photodetector saturation due to strong DC components. To compensate the losses introduced mostly by the MZM, an erbium-doped fiber amplifier (EDFA) is inserted to boost the pulse power as much as possible but avoiding the onset of modulation instability. The amplified spontaneous emission noise (ASE) introduced by the EDFA is removed by a reflective fiber Bragg grating (FBG) filter, centered at λ_0, before launching the pulses into the fiber under test (FUT). The backscattering signal $E(t)$ generated by the FUT, whose spectrum still exhibits a double sideband modulation, is amplified by a second EDFA at the receiver front-end, followed by a narrow band (NB) optical filter. The bandwidth of the NB filter is tuned to suppress one of the chirped sidebands (with a high rejection of more than 30 dB) and the ASE. Note that while the choice of which sideband must be suppressed is irrelevant for the method, their chirp rate shows opposite sign thus affecting the sign of the results if not properly taken into account. Finally, a 12 GHz photodetector (PD), followed by an oscilloscope (OSC) triggered by the AWG is used to collect the received traces $I(t)$. Such traces are directly low-pass filtered by the OSC with a cut-off frequency $f_{LPF} = 9.5$ GHz to remove high-frequency noise. The decision of inserting the NB filter at the end of the setup was taken after observing that no gain reduction was induced in the first EDFA when both sidebands of the input pulse were being amplified. This solution allowed to minimize the total amount of ASE reaching the PD, thus improving the received signal quality.

The FUT consists of a standard single-mode optical fiber of length $L_{\mathrm{FUT}} \cong 100$ m which incorporates aluminum alloy wires running in parallel to the fiber. The wires can be made accessible in various points where the FUT can be heated up

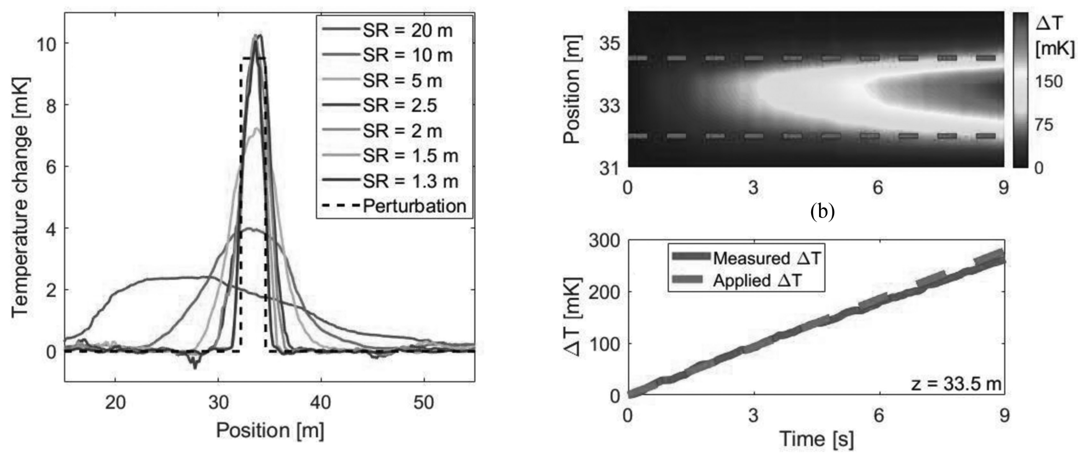

Fig. 3. (a) Temperature changes measured for different spatial resolutions with fixed overlap factor $F = 7$. The black dashed line represents the applied temperature change. (b) Temperature change measured over a temporal interval of 9 seconds (using $N = 10$ and $F = 7$). The red dashed lines identify the heated fiber section of length L_p. (c) Comparison between the measured temperature change magnitude with respect to the applied one.

through Joule effect by applying a voltage V_{FUT} between any two accessible points. The fiber-wire bundle is covered by a thick polymeric coating that allows for partial isolation from external perturbations, thus ideally securing a uniform and efficient temperature change. The temperature changes in the fiber as a function of the current are calibrated using standard CP phase sensitive reflectometry methods [18].

IV. Results

To experimentally demonstrate the spatial resolution improvement provided by sub-bands processing, a segment of the FUT of length $L_p = 2.5$ m, centered at position $z = 33.5$ m, has been heated up uniformly by applying a constant voltage $V_{\text{FUT}} = 1.2$ V to the metallic wires attached to the FUT. The oscilloscope is set to acquire 2^{14} traces at a rate R, monitoring the perturbation acting on the fiber for about 9 seconds. To smooth down fast environmental changes that could reduce the quality of the correlation operation in (14), the traces collected every three consecutive acquisitions have been averaged, limiting the effective measurement rate to $R_{eff} \cong 550$ Hz. To secure a visible temperature change, two arbitrary traces separated by $\delta t = 0.24$ s, have been selected as $I_r(t)$ and $I_m(t)$, and the corresponding passband terms $I_{pb,r}(f)$ and $I_{pb,m}(f)$ have been extracted with a digital rectangular passband filter of width $\delta\upsilon$. Finally, the overlap factor has been set to $F = 7$ based on the optimization process described in Section V.

The proposed method has then been executed for different values of $N = [1,\ 2,\ 4,\ 8,\ 10,\ 13,\ 15]$,corresponding to spatial resolutions of $SR = [20,\ 10,\ 5,\ 2.5,\ 2,\ 1.5,\ 1.3]$ m and a total number of sub-bands $\tilde{N} = [1,\ 8,\ 22,\ 50,\ 64,\ 85,\ 99]$. Results are shown in Fig. 3(a), where we can see that, for the values of $N < 8$, corresponding to spatial resolutions larger than $L_p = 2.5$ m, the measured results show a hot-spot with distorted magnitude, spread over a section of the fiber proportional to the spatial resolution. In these cases, the longitudinal shift Λ of the local pattern of the backscattering trace $I^n_{pb,m}(t)$ occupies at most a fraction of the correlation window $\widetilde{\tau}_c$. Consequently, no improvement in the spatial resolution can be observed in Fig. 3(a) for $N < 8$, resulting in a temperature change profile having a distorted hot-spot. This effect can be especially observed for values of $N \leq 4$, when the amplitudes and the full-width at half-maximum of the measured hot-spot are visibly different from the applied temperature change (represented in the figure by the black dashed line). For values of $N \geq 8$, however, the size of the correlation window $\widetilde{\tau}_c$ is equal or shorter than the perturbed segment L_p. Hence, the temporal correlation in (14) correctly estimates the temperature-induced shifts with an improved spatial resolution. The results of the proposed method agree very well with the real applied temperature change. Observing the lines corresponding to $N \geq 8$ in Fig. 3(a), the effects of the increased spatial resolution can be verified by the sharper transitions in the temperature profile. Finally, Fig. 3(a) also shows that the procedure introduces only a minimal measurement SNR degradation, which can be verified by the small increase in the temperature profile oscillations out of the hot-spot location. This result confirms that the averaging operation between the traces $I^n_{\text{xcorr}}(t)$ computed from overlapped sub-bands is an effective solution for compensating the SNR reduction.

It must be pointed out that the change in the input pulse indeed does not influence the high performance of the standard CP ϕ-OTDR setup such as the robustness to signal fading or the high sensitivity. This can be verified by tracking the temperature change of the fiber section around the position $z = 33.5$ m during the 9 s of acquisition. The results are shown in Fig. 3(b) and 3(c) where a linearly growing temperature change around the hot-spot can be observed over time without distortion or signal loss. For this measurement $N = 15$ has been chosen, thus securing a spatial resolution of $SR = 1.3$ m. As can be seen, the magnitude of the measured ΔT closely follows the applied perturbation and the position of the hot-spot is correctly identified, spread over a fiber section of length L_p.

To compare the advantages in monitoring long perturbations obtained by the sub-bands processing with respect to the original

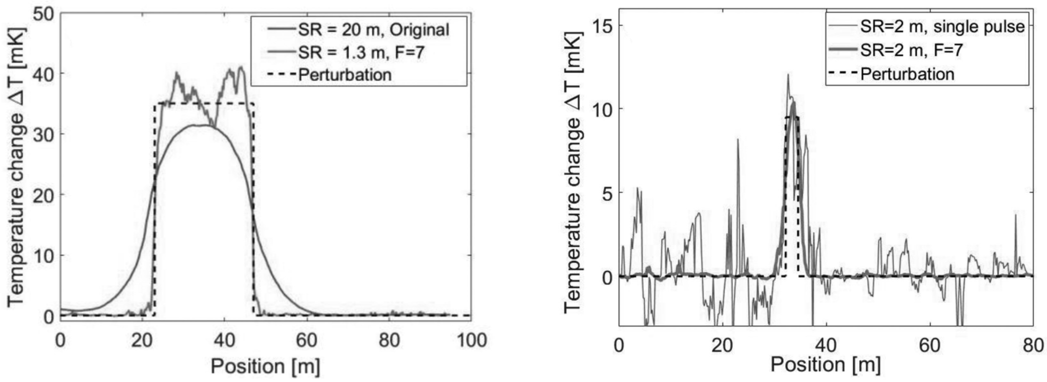

(a) (b)

Fig. 4. (a) Temperature change over 25 meters measured with the original chirped-pulse ϕ-OTDR method (SR $=$ 20 meter) (blue line) and with the proposed high resolution method ($N = 10 \rightarrow SR = 2$ m, $F = 7$) (red line). (b) Comparison between the temperature profile measured with the original method and pulses of $\tau_p = 20$ ns, providing a spatial resolution $SR = 2$ m (blue line) and the temperature profile measured with the proposed high resolution method using pulses of $\tau_p = 200$ ns and setting $N = 10$, thus $SR = 2$ m and $F = 7$.

CP ϕ-OTDR, a temperature change has been induced on a fiber segment of length $L_p = 25$ m, centered around the position $z = 37$ m. As before, the temperature change has been generated through Joule heating of the metallic wires. However, to guarantee a visible perturbation over such a long fiber segment, the applied voltage has been raised up to $V_{\rm FUT} = 8$ V. The traces have been first collected using the standard CP ϕ-OTDR setup, sending pulses of width $\tau_p = 200$ ns to provide a spatial resolution of $SR = 20$ m. After the acquisition, the power supply was turned off to let the fiber cool down to room temperature before turning it on again and measure with the proposed high-resolution setup. The measurement results obtained by both systems are shown in Fig. 4(a), where the blue line represents the temperature profile extracted with the standard setup, while the red one represents the high-resolution curve obtained through sub-bands processing. The reference and measurement traces have been separated by $\delta t = 0.24$ s in the two cases and a value of $N = 15$ has been chosen. As can be seen, the results obtained from both setups correctly identify the position and the magnitude of the perturbation but, as expected, the transients of the trace computed from the original CP ϕ-OTDR are much longer than the transients of the trace extracted by applying sub-bands processing. Moreover, the increased spatial resolution allows a more accurate evaluation of the perturbation affecting the fiber. In particular, the trace obtained by applying sub-bands processing highlights a non-uniform temperature profile along the perturbed fiber section, which is hidden in the standard setup by its low spatial resolution. The high-resolution trace exhibits a 2-fold reduction in the SNR evaluated outside the hot-spot region, compared to the trace measured with the original setup. Nevertheless, such an SNR reduction has only a negligible impact on the results quality.

A final demonstration of the performance improvement provided by the proposed method has been realized by comparing the measurements of a $L_p = 2.5$ m-long temperature change obtained by a standard CP ϕ-OTDR with a 2 m spatial resolution and the proposed method with the same resolution. For this, a standard CP ϕ-OTDR has been implemented using pulses of $\tau_p = 20$ ns and a total applied chirp of $\delta\upsilon = 0.4$ GHz. The proposed high-resolution CP ϕ-OTDR has been however implemented with much longer pulses of $\tau_p = 200$ ns, chirp of $\delta\upsilon = 4$ GHz, and $N = 10$ sub-bands, securing the same spatial resolution of $SR = 2$ m. As can be seen in Fig. 4(b), the temperature profile measured with sub-bands processing exhibits a much higher measurement quality compared to the one obtained by the standard setup. Indeed, while the measured temperature change matches the applied perturbation in both cases, the measurement with the standard setup shows high-amplitude spikes caused in the cross-correlation process due to the low measurement SNR. This way, result clearly demonstrates the significant improvement provided by the setup and sub-band processing proposed.

V. Overlap Factor Optimization

Section II described the technique proposed in this paper based on the extraction of overlapped sub-bands from the spectrum $I_{pb}(f)$, followed by an averaging process to mitigate the consequent SNR reduction. To extract overlapped sub-bands, the central frequency of the applied digital passband filter is shifted in steps of $\delta W = \Delta W/F$, where F is an integer number called overlap factor. Using then a factor $F > 1$ results in $\tilde{N} = F(N-1)+1 > N$ overlapped sub-bands. Assuming the noise affecting $I_{pb}(f)$ to be white, for $F = 1$ the N independent sub-bands will all have uncorrelated noise. This can secure the maximum efficiency in the averaging process described in (15), to reduce the error in the estimation of the shifts $\Lambda(\mathrm{t})$. Using large values of F, a high number of windows can be exploited for averaging; however, the noise affecting overlapped sub-bands becomes progressively more correlated and the efficiency of the averaging process is reduced. A high value of F will not then proving any benefit. Nevertheless, low values of F still guarantee significant SNR mitigation gains. This is clearly represented in Fig. 5(a), which shows the retrieved temperature profile over an unperturbed fiber section (i.e., the impact of the system noise) for different overlap factors F. Fig. 5(b) shows the temperature

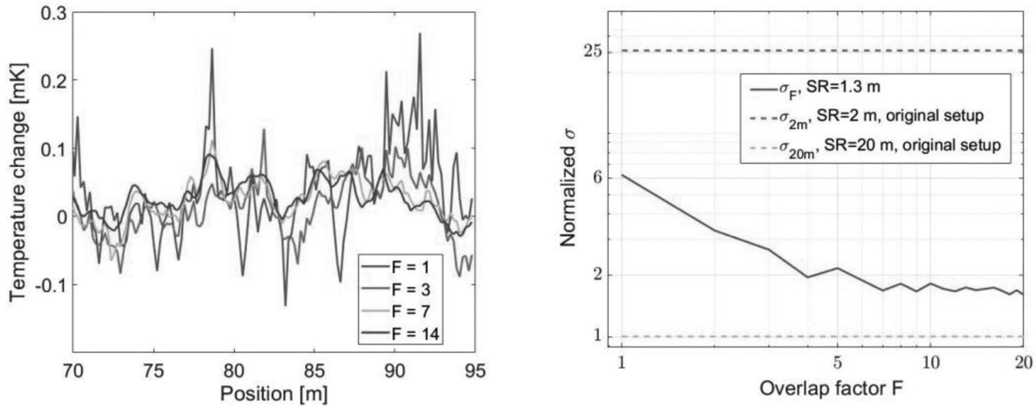

(a) (b)

Fig. 5. (a) Comparison between the unperturbed sections of the fiber measured for different values of F; (b) Normalized standard deviation σ for different values of F compared with the normalized standard deviations of the original setup with different spatial resolutions.

standard deviation measured over fiber locations out of the applied hot-spot, showing a strong reduction of the temperature noise when increasing F from 1 to 7. The improvement is however significantly reduced when F is increased to 14. The total chirp δv applied to the pulse affects the overlap factor, since for a given F a larger chirp implies a larger bandwidth of the K sub-bands and a lower noise correlation. To achieve the highest SNR mitigation gain, the optimal value of F must then be identified every time the pulse parameters are changed. However, often the value of $F = 7$ can be considered a default considering that the complexity of the algorithm increases for increasing values of F and that the normalized standard deviation does not change significantly beyond that value.

The easiest way to identify the optimum value of the overlap factor consists in computing the noise standard deviation σ of the retrieved temperature profile as a function of F. The data represented in Fig. 4(a) are used to perform this analysis, in order to allow a comparison of the σ achieved with our technique with respect to the original setup. For our setup, the overlap factor F has been varied from 1 to 20 and the σ_F have been computed in the short unperturbed fiber section $S = [70,\ 95]$ m since, as can be seen in Fig. 5(a), the noise evolves over lengths much shorter than the spatial resolution and the high spatial sampling guarantees a sufficiently accurate estimation. For the original setup, where the input pulse width has been set to $\tau_p = 200$ ns to provide a $SR = 20\ m$, the standard deviation $\sigma_{20\text{m}}$ is computed over the same section S. The σ_F have been normalized then to $\sigma_{20\text{m}}$ to highlight the SNR reduction introduced by our technique with respect to the original system. As can be seen in Fig. 5(b), the σ_F show a decreasing behavior for increasing values of F, which corresponds to a progressively stronger mitigation of the SNR reduction. The curve saturates at a mean value of 1.77 after $F = 7$, proving that the proposed method may achieve a significant SR improvement at the cost of a SNR reduction lower than a factor 2 with respect to the original setup. Since an overlap factor greater than $F = 7$ does not provide any further improvement, it can be considered as the optimal one for the chosen parameters. For the sake of comparison, the normalized standard variation of the noise $\sigma_{2\text{m}}$ of the original setup when a pulse of width $\tau_p = 20$ ns, $SR = 2$ m, is used (data represented in Fig. 4(b)) is added to Fig. 5(b). As can be seen, in such a case our technique guarantees better performance even without using overlapped sub-bands.

VI. Conclusion

In this paper, a method to improve the spatial resolution of CP ϕ-OTDR systems based on sub-bands processing has been proposed and experimentally demonstrated. The division of the fiber response to the chirped pulse into spectral sub-bands, and the consequent processing, allows to convert a measurement performed with a long pulse (and hence a low spatial resolution), in a measurement with high spatial resolution at the cost of a slightly reduced SNR (less than a factor 2 in our demonstration). The reduced pulse width caused by the sub-band processing, proportionally limits the maximum shot-to-shot measurable temperature or strain gradient. However, for the trigger rates and chirp bandwidths used in this work this range reduction still allow measuring the vast majority of physical processes of interest (e.g., intrusions, small seismic features, etc.). Note that in all cases, the actual measurement range can exceed substantially that one allowed by the chirp bandwidth, simply by using temporally adjacent traces and keeping track of the previous measurements [24]. Note also that to avoid distortions in the linear chirp generated by the MZM, the intensity of the driving signal generated by the AWG has to be reduced, limiting the magnitude of the generated chirped sidebands and consequently the maximum measurement range. By implementing more precise techniques to realize the sidebands or by finding a different way to add the carrier to the input pulse, without increasing the phase noise, such limitation can be further relaxed.

References

[1] T. M. Daley, B. M. Freifeld, J. Ajo-Franklin, and S. Dou, "Field testing of fiber-optic distributed acoustic sensing (DAS) for subsurface seismic monitoring," *Leading Edge*, vol. 32, no. 6, pp. 699–706, Jun. 2013.

[2] L. Schenato *et al.*, "Distributed optical fibre sensing for early detection of shallow landslides triggering," *Sci. Rep.*, vol. 7, no. 1, Oct. 2017, Art. no. 14686.

[3] H. F. Martins, S. Martin-Lopez, P. Corredera, J. D. Ania-Castañon, O. Frazão, and M. Gonzalez-Herraez, "Distributed vibration sensing over 125 km with enhanced SNR using phi-OTDR over a urfl cavity," *J. Lightw. Technol.*, vol. 33, no. 12, pp. 2628–2632, Jun. 2015.

[4] L. Marcon, A. Galtarossa, and L. Palmieri, "High-frequency high-resolution distributed acoustic sensing by optical frequency domain reflectometry," *Opt. Express*, vol. 27, no. 10, May 2019, Art. no. 13923.

[5] J. C. Juarez, E. W. Maier, K. N. Choi, and H. F. Taylor, "Distributed fiber-optic intrusion sensor system," *J. Light. Technol.*, vol. 23, no. 6, Jun. 2005, Art. no. 2081.

[6] H. F. Martins, S. Martin-Lopez, P. Corredera, P. Salgado, O. Frazão, and M. González-Herráez, "Modulation instability-induced fading in phase-sensitive optical time-domain reflectometry," *Opt. Lett.*,vol. 38, no. 6, pp. 872–874, Mar. 2013.

[7] Z. He, Q. Liu, X. Fan, D. Chen, S. Wang, and G. Yang, "Fiber-optic distributed acoustic sensors (DAS) and applications in railway perimeter security," *Proc. SPIE*, vol. 10821, Oct. 2018, Art. no. 1082102.

[8] L. Costa *et al.*, "Fast and direct measurement of the linear birefringence profile in standard single-mode optical fibers," *Opt. Lett.*, vol. 45, no. 3, pp. 623–626, Jan. 2020.

[9] P. Healey, "Fading in heterodyne OTDR," *Electron. Lett.*, vol. 20, no. 1, pp. 30–32, Jan. 1984.

[10] T. Zhu, Q. He, X. Xiao, and X. Bao, "Modulated pulses based distributed vibration sensing with high frequency response and spatial resolution," *Opt. Express*, vol. 21, no. 3, pp. 2953–2963, Feb. 2013.

[11] Y. Muanenda, C. J. Oton, S. Faralli, and F. D. Pasquale, "A cost-effective distributed acoustic sensor using a commercial off-the-shelf DFB laser and direct detection ϕ-OTDR," *IEEE Photon. J.*, vol. 8, no. 1, pp. 1–10, Feb. 2016.

[12] M. A. Soto, J. A. Ramírez, and L. Thévenaz, "Intensifying the response of distributed optical fibre sensors using 2D and 3D image restoration," *Nat. Commun.*, vol. 7, Mar. 2016, Art. no. 10870.

[13] J. Pastor-Graells, H. F. Martins, A. Garcia-Ruiz, S. Martin-Lopez, and M. Gonzalez-Herraez, "Single-shot distributed temperature and strain tracking using direct detection phase-sensitive OTDR with chirped pulses," *Opt. Express*, vol. 24, no. 12, Jun. 2016, Art. no. 13121.

[14] B. Lu *et al.*, "High spatial resolution phase-sensitive optical time domain reflectometer with a frequency-swept pulse," *Opt. Lett.*, vol. 42, no. 3, pp. 391–394, Feb. 2017.

[15] M. R. Fernández-Ruiz, J. Pastor-Graells, H. F. Martins, A. Garcia-Ruiz, S. Martin-Lopez, and M. Gonzalez-Herraez, "Laser phase-noise cancellation in chirped-pulse distributed acoustic sensors," *J. Light. Technol.*, vol. 36, no. 4, pp. 979–985, Feb. 2018.

[16] D. Chen, Q. Liu, X. Fan, and Z. He, "Distributed fiber-optic acoustic sensor with enhanced response bandwidth and high signal-to-noise ratio," *J. Light. Technol.*, vol. 35, no. 10, pp. 2037–2043, May 2017.

[17] D. Chen, Q. Liu, Y. Wang, H. Li, and Z. He, "Fiber-optic distributed acoustic sensor based on a chirped pulse and a non-matched filter," *Opt. Express*, vol. 27, no. 20, Sep. 2019, Art. no. 29415.

[18] J. J. Mompó, L. Shiloh, N. Arbel, N. Levanon, A. Loayssa, and A. Eyal, "Distributed dynamic strain sensing via perfect periodic coherent codes and a polarization diversity receiver," *J. Light. Technol.*, vol. 37, no. 18, pp. 4597–4602, Sep. 2019.

[19] S. Liehr, S. Münzenberger, and K. Krebber, "Wavelength-scanning coherent OTDR for dynamic high strain resolution sensing," *Opt. Express*, vol. 26, no. 8, pp. 10573–10588, Apr. 2018.

[20] 1. D. Chen, Q. Liu, and Z. He, "High-fidelity distributed fiber-optic acoustic sensor with fading noise suppressed and sub-meter spatial resolution," *Opt. Express*, vol. 26, no. 13, pp. 16138–16146, Jun. 2018.

[21] L. Marcon, M. A. Soto, M. Soriano-Amat, L. Costa, H. F. Martins, L. Palmieri, and M. Gonzalez-Herraez, "Boosting the spatial resolution in chirped pulse ϕ-OTDR using sub-band processing," in *Proc. 17h Eur. Workshop Opt. Fibre Sensors*, 2019, vol. 11199, Art. no. 111991W.

[22] J. S. Sirkis and H. W. Haslach, "Interferometric stain measurement by arbitrarily configured surface-mounted, optical fibers," *J. Light. Technol.*, vol. 8, no. 10, pp. 1497–1503, Oct. 1990.

[23] Y. Koyamada, M. Imahama, K. Kubota, and K. Hogari, "Fiber-optic distributed strain and temperature sensing with very high measurand resolution over long range using coherent OTDR," *J. Light. Technol.*, vol. 27, no. 9, pp. 1142–1146, May 2009.

[24] H. D. Bhatta *et al.*, "Dynamic measurements of 1000 microstrains using chirped-pulse phase-sensitive optical time-domain reflectometry," *J. Light. Technol.*, vol. 37, no. 18, pp. 4888–4895, Sep. 2019.